Ilamycins are dual inhibitors of ClpX and ClpC1 involved in proteostasis in Mycobacteria

Yamin Gao[1,2,3,4#], Cuiting Fang[1,2,3,4#], Biao Zhou[1,5,6], H.M. Adnan Hameed[1,2,3,4], Changli Sun[3,7], Xirong Tian[1,2,3,4], Jing He[1,2,4,8], Xingli Han[1,2,3,4], Han Zhang[1,2,4,9], Jianhua Ju[3,7], Xinwen Chen[6], Nanshan Zhong[6], Junying Ma[3,7*], Xiaoli Xiong[1,2,3,6*], Tianyu Zhang[1,2,3,4,6*]

[1] State Key Laboratory of Respiratory Disease, Guangzhou Institutes of Biomedicine and Health, Chinese Academy of Sciences, Guangzhou 510530, China

[2] Guangdong-Hong Kong-Macao Joint Laboratory of Respiratory Infectious Diseases, Guangzhou Institutes of Biomedicine and Health, Chinese Academy of Sciences, Guangzhou 510530, China

[3] University of Chinese Academy of Sciences, Beijing 100049, China

[4] China-New Zealand Joint Laboratory on Biomedicine and Health, Guangzhou Institutes of Biomedicine and Health, Chinese Academy of Sciences, Guangzhou 510530, China

[5] Guangzhou Medical University, Guangzhou 510180, China

[6] Guangzhou National Laboratory, Guangzhou 510005, China

[7] CAS Key Laboratory of Tropical Marine Bio-Resources and Ecology, Guangdong Key Laboratory of Marine Materia Medica, RNAM Center for Marine Microbiology, South China Sea Institute of Oceanology, Chinese Academy of Sciences, Guangzhou 510301, China.

[8] Institute of Physical Science and Information Technology, Anhui University, Hefei 230601, China

[9] School of Life Sciences, University of Science and Technology of China, Hefei 230026, China

[#] These authors contributed equally to this work.

[*]Corresponding authors: Tianyu Zhang (Tel: +86-20-32015270, E-mail: zhang_tianyu@gibh.ac.cn); Xiaoli Xiong (Tel:+8617815390976, E-mail: xiong_xiaoli@gibh.ac.cn); Junying Ma (Tel: +86-20-34066449, Email: majunying@scsio.ac.cn).

Abstract

Combatting drug-resistant *Mycobacterium tuberculosis* (Mtb) necessitates the discovery of novel anti-Mtb agents targeting unexploited molecular pathways. The Clp protease system, integral to protein homeostasis in Mtb, has emerged as a promising target. We report that ilamycins exhibit potent antimycobacterial activity by specifically targeting ClpX and ClpC1. Spontaneous resistance to ilamycin E (ILE) and ilamycin F (ILF) in Mtb mutants correlated with mutations in ClpC1 and ClpX. Molecular docking simulations suggest these mutations occur at critical residues in the N-terminal domain (NTD) of MtbClpC1 and MtbClpX. Functional analyses, including gene over-expression in *Mycobacterium marinum* and targeted gene editing in *Mycobacterium abscessus* (Mab) and *Mycobacterium smegmatis* (Msm), substantiated the significance of these mutations in conferring ILE and ILF resistance. Gene silencing heightened the susceptibility of recombinant Mab and Msm strains to ILE and ILF, concurrently impairing their growth. Differential scanning fluorimetry confirmed the stabilization of MtbClpC1-NTD by ILE and ILF. Moreover, ILE markedly impeded the proteolytic function of the ClpC1P1P2 complex without diminishing ClpC1 ATPase activity. Collectively, our findings demonstrate that ilamycins exert mycobactericidal effects by disrupting ClpC1 and ClpX functions, leading to proteostasis dysregulation. This study underscores the therapeutic potential of targeting the Clp protease system in the treatment of tuberculosis.

Introduction

Tuberculosis (TB), caused by *Mycobacterium tuberculosis* (Mtb), is among the most lethal bacterial infections worldwide, accounting for over 1.4 million fatalities annually[1]. Despite the availability of treatments, TB remains a major public health threat on a global scale, aggravated by the proliferation of drug-resistant strains, including multidrug-resistant, extensively drug-resistant, and total drug-resistant Mtb[2,3]. Furthermore, infections caused by nontuberculous mycobacteria (NTM) are on the rise, presenting significant clinical challenges due to their inherent resistance to many available antibiotics[4]. NTM infections lead to serious respiratory, dermatological, and mucosal conditions, particularly in immunocompromised individuals[5]. Therefore, discovery and development of drugs of novel molecular mechanisms with efficacy against drug-resistant mycobacteria are urgently needed for the management of mycobacterial diseases.

Mycobacterial Clp proteases, vital multi-subunit protein complexes involved in intracellular protein degradation, are emerging as promising therapeutic targets[6-9]. The Clp proteases are composed of ClpP1 and ClpP2 peptidases, and an ATP-dependent AAA+ unfoldase (ClpX or ClpC1)[9]. In mycobacteria, ClpP1 and ClpP2 form homo-heptameric rings that subsequently assemble into an active hetero-tetradecamer protease. ClpX and ClpC1, each forming homo-hexameric rings, associate with ClpP2 to facilitate protein unfolding and translocation into the protease chamber via ATP hydrolysis[10,11]. Indispensable for mycobacterial survival[9,12,13], these enzymes not only maintain intracellular protein quality but also modulate responses to environmental stressors and contribute to the pathogenicity of virulent strains[7,14].

Ilamycins, also known as rufomycins, are a group of cycloheptapeptides synthesized by *Streptomyces atratus* SCSIO ZH16 derived from the South China Sea[15]. These compounds, particularly ilamycin E (ILE) and ilamycin F (ILF), have demonstrated potent activity against Mtb H37Rv[15]. Despite their promising anti-Mtb properties, the mode of action of ilamycins, the activity against NTM and other non-mycobacteria pathogenic bacteria, and potential drug interactions are still unknown.

52 Moreover, the efficacy of ilamycins in macrophages and against drug-resistant clinical
53 Mtb strains is yet to be elucidated. In this study, we comprehensively investigated the
54 mechanism of action of ilamycins and examined their activity extensively.
55

Results

Selective and potent *in vitro* and *ex vivo* antibacterial activity of ILE and ILF

ILE exhibited strong inhibitory effects on Mtb, *Mycobacterium marinum* (Mmr), *Mycobacterium abscessus* (Mab), and *Mycobacterium smegmatis* (Msm) (Table 1), while ILF was notably active against Mtb, Mmr, and Msm, with less pronounced activity against Mab. This variation in efficacy may be attributed to structural differences between ILE and ILF (Fig. 1) and the distinct cell wall permeabilities of the mycobacterial species[16,17]. The minimal inhibitory concentrations (MICs) of ILE to $H_{37}Rv$ and clinically isolated drug-resistant Mtb strains ranged from 0.01 to 0.05 μg mL^{-1}, consistent with that of the laboratory standard Mtb $H_{37}Rv$ strain (0.05 μg mL^{-1}). Synergistic effects were observed when ILE was combined with rifampicin (RIF) or the new anti-TB drug TB47 currently in the preclinical stage[18], and ILF with isoniazid (INH) or TB47, while partial synergy was noted when ILE combined with INH and ILE with ethambutol (EMB). Additive effects were seen when ILE combined with streptomycin (STR), ILF with EMB, and ILF with STR. No antagonism was observed between any of the drugs selected and ILE or ILF. In mouse RAW264.7 macrophage, ILE effectively inhibited autoluminescent Mtb H37Rv (AlRv, MIC, 0.2 μg mL^{-1}). However, neither ILE nor ILF showed activity against common non-mycobacterial clinical isolates, such as *Staphylococcus aureus*, *Acinetobacter baumannii*, *Enterococcus faecium*, *Klebsiella pneumoniae*, and *Pseudomonas aeruginosa* (MICs > 128 μg mL^{-1}).

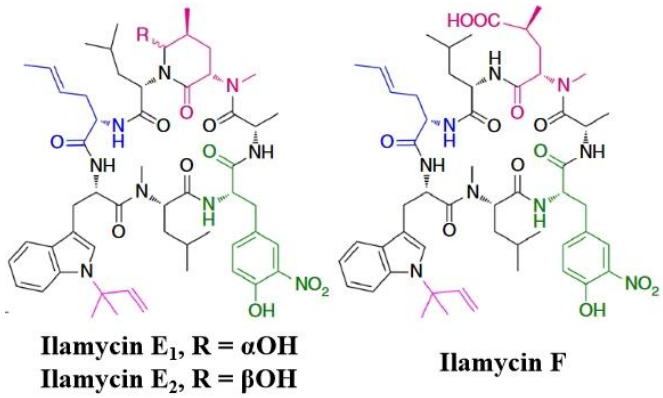

Fig. 1 | The structure of ilamycin E and ilamycin F.

Table 1 | Ilamycin E and ilamycin F spectrum of activities

Strains	ILE MIC (μg mL^{-1})	ILF MIC (μg mL^{-1})
AlRa	0.05[a]	1.25[a]
AlRv	0.05[a]	-
AlMsm	0.0625[a]	2.5[a]
AlMab	1[a]	20[a]
AlMmr	0.08[a]	0.625[a]
$H_{37}Rv$	0.025[b]	2.5[b]
K11*	0.025-0.05[b]	-
K12*	0.025[b]	-
K13*	0.01[b]	-
K14*	0.01[b]	-
K16*	0.05[b]	-
K17*	0.01[b]	-
K18*	0.025-0.05[b]	-
K19*	0.01[b]	-
K20*	0.05[b]	-
Staphylococcus aureus	> 128	> 128
Acinetobacter baumannii	> 128	> 128
Enterococcus faecium	> 128	> 128
Klebsiella pneumoniae	> 128	> 128
Pseudomonas aeruginosa	> 128	> 128

AlRa, autoluminescent Mtb $H_{37}Ra$; AlRv, autoluminescent Mtb $H_{37}Rv$; AlMsm, autoluminescent Msm; AlMab, autoluminescent Mab; AlMmr, autoluminescent Mmr; *, clinical resistant Mtb; [a], MICs obtained by detection of relative light units; [b], MICs obtained by the microplate alamar blue assay (MABA) method.

Mutation patterns of *clpC1* and/or *clpX* in ILE- or ILF-resistant Mtb, Mab, Msm, and Mmr strains

We screened and isolated spontaneously generated mutants resistant to ILE or ILF. The spontaneous mutation rate screened for ILE-resistant Mtb at 0.5 μg mL^{-1} was approximately 2.5×10^{-9}, notably lower than the rates for RIF or INH[19]. Whole genome sequencing (WGS) revealed predominant mutations at P30 of ClpX and F80 of ClpC1 in ILE-resistant Mtb strains (Table 2). Whereas, ILE-resistant Mab had mutations at the same site in ClpX and different sites in ClpC1, including F2, Q17, H77, L88, an insertion leading to an M1-FERF-F2 sequence (Table 2). However, ILE-resistant Mmr strains carried mutations exclusively in ClpC1, with no alterations in ClpX (Table 2). Similarly, ILF-resistant Msm mutants showed mutations only in ClpC1, at F2, F5, F80, L88, I197, and an insertion between M1 and F2 (Table 2), respectively. Cross-resistance was observed between ILE and ILF, with all ILE-resistant Mab strains showing resistance to ILF and vice versa for ILF-resistant Msm strains. These findings suggest that both ILE and ILF may target the ClpX and ClpC1 proteases.

95 **Table 2 | Mutations of ClpC1 and ClpX in ILE- and ILF-resistant mutants**

Strains No.	Drug/MICs (μg mL^{-1})	Mutation in ClpC1	Mutation in *clpC1*	Mutation in ClpX	Mutation in *clpX*
Mtb$^{R1\#}$	ILE 0.625	-	-	P30H	CCC→CAC
Mtb$^{R2\#}$	ILE 20	F80I	TTT→ATT	P30H	CCC→CAC
Mtb$^{R3\#}$	ILE 20	F80V	TTT→GTT	P30H	CCC→CAC
Mtb$^{R4\#}$	ILE 0.1	F80I	TTT→ATT	-	-
Mtb$^{R5\#}$	ILE 0.1	F80V	TTT→GTT	-	-
Mtb$^{R6\#}$	ILE 0.1	F80L	TTT→CTT	-	-
Mtb$^{R7\#}$	ILE 20	F80C	TTT→TGT	-	-
Mab$^{R1\#}$	ILE > 128 ILF > 128	-	-	P30H	CCC→CAC
Mab$^{R2\#}$	ILE 4 ILF > 128	F2L	TTC→TCC	-	-
Mab$^{R3\#}$	ILE 4 ILF > 128	M1-FERF-F2	Ins: TTCGAGAGATTC	-	-
Mab$^{R4\#}$	ILE 4 ILF > 128	Q17R	CAA→CGA	-	-
Mab$^{R5\#}$	ILE > 128 ILF > 128	H77D	CAC→GAC	-	-
Mab$^{R6\#}$	ILE > 128 ILF > 128	L88R	CTG→CGG	-	-
Mmr$^{R1\#}$	ILE 1 ILF 4	F2L	TTC→TCC	-	-
Mmr$^{R2\#}$	ILE 10 ILF 40	H77D	CAC→GAC	-	-
Mmr$^{R3\#}$	ILE 10 ILF 40	L88R	CTC→CGC	-	-
Msm^{R1*}	ILE 0.5 ILF 20	F2S	TTT→TCT	-	-
Msm^{R2*}	ILE 0.25 ILF 10	F2C	TTT→TGT	-	-
Msm^{R3*}	ILE 1 ILF 20	M1-L-F2	Ins: GTT	-	-
Msm^{R4*}	ILE 1 ILF 10	F5I	TTT→ATT	-	-
Msm^{R5*}	ILE 0.5 ILF 40	F80S	TTC→TCC	-	-
Msm^{R6*}	ILE 0.25 ILF 10	L88P	CTC→CCC	-	-
Msm^{R7*}	ILE 0.25 ILF 20	L88R	CTC→CGC	-	-

Msm^{R8*}	ILE 0.25 ILF 10	F2S; I197N	TTT→TCT; ATC→AAC	-	-

#, Resistant mutants were selected from ILE-containing plates; *, Resistant mutants were selected from ILF-containing plates; Ins, insertion; Underlines indicate mutated bases; - showed no mutation.

Molecular docking simulation between ILE and MtbClpC1-N-terminal domain (MtbClpC1-NTD) as well as MtbClpX-NTD

Through molecular docking, we simulated the interaction between ILE and the MtbClpC1-NTD (Fig. 2a) as well as the MtbClpX-NTD (Fig. 2b). The simulations identified key binding residues within MtbClpC1-NTD and MtbClpX-NTD, aligning with mutation sites such as Q17, H77, F80, and L88 in ClpC1-NTD, and the P30 in MtbClpX-NTD. Given the structural similarities between ILE and ILF, and their observed cross-resistance, we did not perform separate docking simulations for ILF. The docking outcomes support the hypothesis that both ILE and ILF target ClpC1 and ClpX.

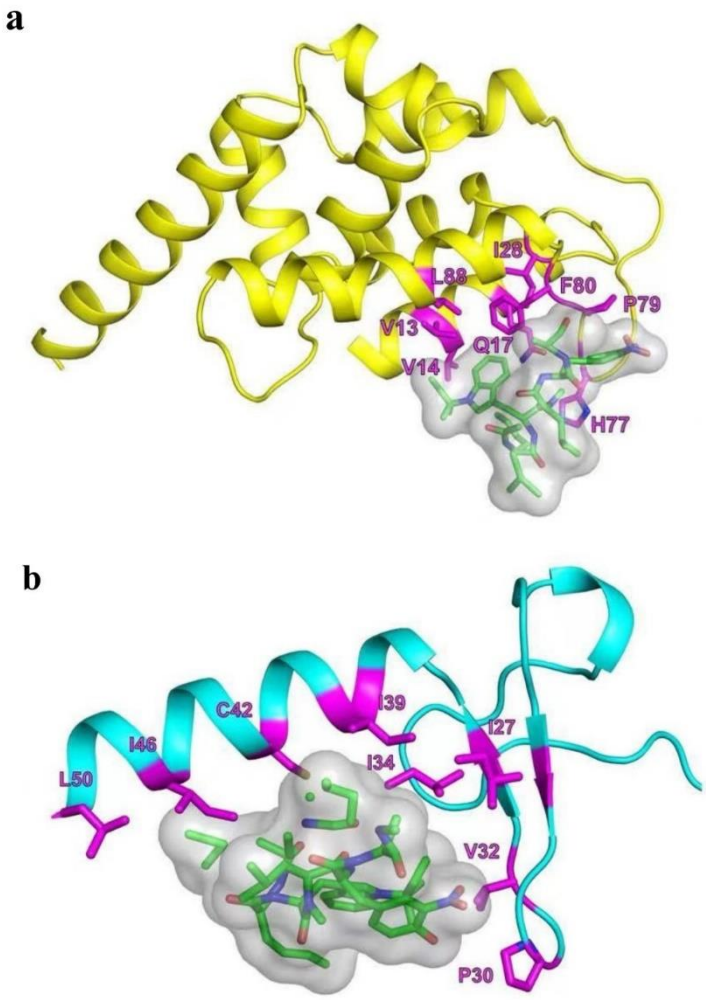

Fig. 2 | The graphical representation of crucial residues in the interaction between ILE and MtbClpC1-NTD as well as MtbClpX-NTD. a Crucial residues in the interaction between ILE and MtbClpC1-NTD. **b** Crucial residues in the interaction between ILE and MtbClpX-NTD. MtbClpC1-NTD, N-terminal domain of Mtb-ClpC1 (residues 1–145); MtbClpX-NTD, N-terminal domain of Mtb-ClpX (residues 1–112).

Resistance to ILE and ILF detected in *clpC1* or *clpX* edited Mab and Msm

We obtained 4 gene-edited strains successfully, 2 in Mab (wild-type ClpC1 ($ClpC1^{wt}$) to $ClpC1^{F2L}$; $ClpX^{wt}$ to $ClpX^{P30H}$) and 2 in Msm ($ClpC1^{wt}$ to $ClpC1^{M1\text{-}L\text{-}F2}$; $ClpC1^{wt}$ to $ClpC1^{I197N}$) (Table 3) by CRISPR/Cpf1-mediated gene editing[20,21]. These edited strains exhibited different resistance levels (Table 3). Notably, the $ClpX^{wt}$ to $ClpX^{P30H}$ mutation in Mab conferred the highest resistance level , with MICs exceeding 128 μg mL^{-1} for ILE and ILF. The $ClpC1^{wt}$ to $ClpC1^{F2L}$ mutation in Mab resulted in a

119 lower resistance increase, with an 8-fold MIC increase for ILE compared to the parent
120 strain. In Msm, the ClpC1^{wt} to ClpC1$^{M1-L-F2}$ mutation raised the MICs of ILE and ILF
121 to 4 and 6.4 times that of the wild-type strains, respectively, while the ClpC1^{wt} to
122 ClpC1^{I197N} mutation did not affect the MICs.

123 **Table 3 | MICs of ILE and ILF to gene edited strains and corresponding spontaneous mutants**

Strains	Amino acid change	ILE MIC (μg mL^{-1})/ (fold change)	ILF MIC (μg mL^{-1})/ (fold change)
Mab^{wt}	/	1	20
Mab$^{R2\#}$	ClpC1^{wt} to ClpC1^{F2L}	4 / (4)	> 128 / (> 6)
Mab-C1^{F2L}	ClpC1^{wt} to ClpC1^{F2L}	8 / (8)	> 128 / (> 6)
Mab$^{R1\#}$	ClpX^{wt} to ClpC1^{P30H}	> 128 / (> 128)	> 128 / (> 6)
Mab-X^{P29H}	ClpX^{wt} to ClpC1^{P30H}	> 128 / (> 128)	> 128 / (> 6)
Msm^{wt}	/	0.0625	2.5
Msm^{R3*}	ClpC1^{wt} to ClpC1$^{M1-L-F2}$	1 / (16)	20 / (8)
Msm-C1$^{M1-L-F2}$	ClpC1^{wt} to ClpC1$^{M1-L-F2}$	0.25 / (4)	16 / (6.4)
Msm^{R8*}	ClpC1^{wt} to ClpC1^{F2S} ClpC1^{wt} to ClpC1^{I197N}	0.25 / (4)	10 / (4)
Msm-C1^{I197N}	ClpC1^{wt} to ClpC1^{I197N}	0.0625 / (1)	2.5 / (1)

$^{\#}$, Resistant mutants were selected from ILE-containing plates. *, Resistant mutants were selected from ILF-containing plates. -C1 or -X means ClpC1 or ClpX was edited.

124 **Sensitivity of Mab, Mmr or Msm overexpressing genes encoding subunit(s) of**
125 **Clp proteases to ILE or ILF**

126 The *clpX*^{wt} and *clpC1*^{wt} genes and their mutant variants were cloned into the extra-
127 chromosome plasmids with different resistance marker, p60A or pMVA
128 (Supplementary Fig. 1), under the strong promoter *hsp60* for overexpression in
129 autoluminescent strains of Mab (AlMab)[22], Msm (AlMsm)[23], and Mmr (AlMmr)[24].
130 Neither overexpression of the wild-type nor mutated ClpC1 (F2L, Q17R, H77D, and
131 L88R) or ClpX (P30H) in AlMab altered sensitivity to ILE. Even concurrent
132 overexpression of all three genes encoding the corresponding subunits (*clpX*, *clpP1*,
133 *clpP2* or *clpC1*, *clpP1*, *clpP2*) in AlMab did not confer ILE resistance. Similarly, in
134 AlMsm, overexpression of either wild-type or mutated ClpC1 (F2S, F2C, F5I, F80S,
135 L88P, and L88R) did not change sensitivity to ILF. In AlMmr, overexpressing ClpC1^{F2L}
136 or ClpC1^{H77D} conferred no resistance to both ILE and ILF. However, AlMmr strain

137 overexpressing ClpC1^{L88R} showed resistance to both ILE and ILF compared to the
138 parent strain (Table 4).

139 **Table 4 | MICs of ILE and ILF to AlMmr strains overexpressing ClpC1 variants**

Strains	ILE MIC (μg mL^{-1}) / (fold change)	ILF MIC (μg mL^{-1}) / (fold change)
AlMmr^{wt}	0.08	0.625
AlMmr::ClpC1^{wt}	0.08 / (1)	0.625 / (1)
AlMmr::ClpC1^{L88R}	0.625 / (8)	5 / (8)
AlMmr::ClpC1^{F2L}	0.08 / (1)	0.625 / (1)
AlMmr::ClpC1^{H77D}	0.08 / (1)	0.625 / (1)

140 **Sensitivity of the *clpX* or *clpC1* gene knocking down Mab or Msm strains to ILE**
141 **or ILF**

142 Knockdown of *clpX* or *clpC1* in Mab (Fig. 3a) or Msm (Fig. 3b) strains resulted in
143 heightened sensitivity to ILE and ILF. When induced with anhydrotetracycline (aTc) in
144 the absence of ilamycins, growth inhibition was observed in both the *clpX* or *clpC1*
145 knockdown strains of Msm and Mab, underscoring the crucial role of these proteins in
146 cellular proliferation. This confirms previous reports of their essentiality in Msm and
147 Mab[25,26].

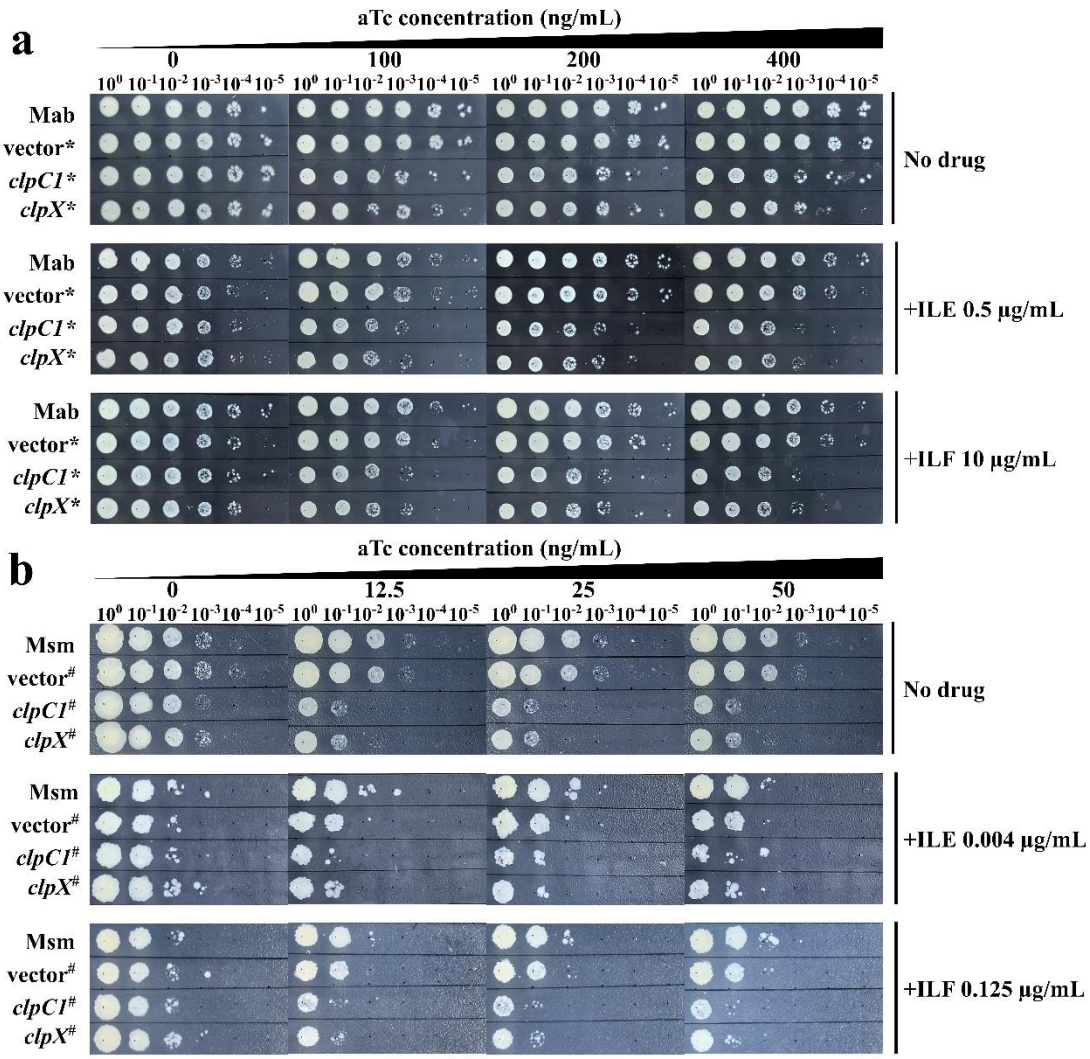

Fig. 3 | Effect of knocking down *clpX* or *clpC1* genes on the sensitivity of Mab and Msm to ILE or ILF. a Effect of knocking down *clpX* or *clpC1* genes on the sensitivity of Mab to ILE or ILF. **b** Effect of knocking down *clpX* or *clpC1* genes on the sensitivity of Msm to ILE or ILF. aTc, anhydrotetracycline, the inducer. *, Mab strains contained different plasmids: vector, the empty plasmid pLJR962; *clpC1,* pLJR962-clpC1 for inducible inhibition of *clpC1* gene; *clpX*, pLJR962-clpX, for inducible inhibition of *clpX* gene. #, Msm strains contained different plasmids: vector, pLJR962, the empty plasmid; *clpC1,* pLJR962-clpC1, for inducible inhibition of *clpC1* gene; *clpX*, pLJR962-clpX, for inducible inhibition of *clpX* gene.

Stablization of NTD of ClpC1 by ILE or ILF

Since all mutations occurred in the NTD of ClpC1 or ClpX in Mtb, Mab, Msm, and Mmr, and due to their identical in NTD sequences (Supplemantary Fig. 2), we specifically expressed and purified the NTD of ClpC1 and ClpX of Mtb, respectively.

Differential scanning fluorimetry (DSF) assay was performed to identify the interactions of ILE or ILF with the purified MtbClpC1-NTD or MtbClpX-NTD. As shown in Fig. 4a, ILE elevated the melting temperature (Tm) of MtbClpC1-NTD from 78.5℃ to 81.5℃, indicating a notable increase in thermal stability (ΔTm of 3℃). On the other hand, ILF increased the thermal stability of the MtbClpC1-NTD slightly with only 1℃ in a thermal shift (Fig. 4b) compared with ILE, which achieved a more evident thermal shift. These results suggested the potential interactions of ILE and ILF with MtbClpC1-NTD. We confirmed that ILE made MtbClpC1-NTD more stable and shifted its melting temperature stronger than ILF did. However, our test results showed that ILE and ILF did not change the dissolution temperature of MtbClpX-NTD (Data not shown).

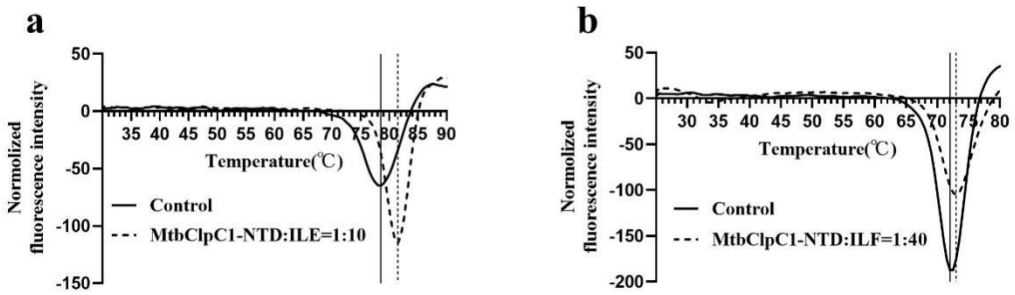

Fig. 4 | The melt curves of MtbClpC1-NTD with ILE and ILF. a The melt curves of MtbClpC1-NTD with ILE. **b** The melt curves of MtbClpC1-NTD with ILF. Control, DMSO; Normalized fluorescence intensity, the fluorescence intensity was normalized to the first time point after exication for each well.

Inhibition of proteolytic activity of the ClpC1P1P2 by ILE but not the proteolytic activity of ClpXP1P2 or the ATPase activity of ClpC1 or ClpX

Considering the superior affinity of ILE with ClpC1 over ILF according to the above results, ILE was selected to represent ilamycins in subsequent biochemical assays. Initial assays evaluated the effect of ILE to the ATP-dependent ATPase activity of ClpC1 and ClpX, revealing no significant alteration in enzyme activity at varying ILE concentrations relative to controls (Supplementary Fig. 3). Subsequent analysis of the effect of ILE to the proteolytic activity of ClpC1P1P2 or ClpXP1P2 complex was

185 assessed by hydrolysis of the model substrate FITC-casein or GFP-SsrA, respectively.
186 ILE substantially inhibited the proteolytic capabilities of the ClpC1^{wt}P1P2 complex to
187 degrade casein with a significant difference as compared to the control group ($P < 0.05$
188 for 1, and $P < 0.0001$ for 10 and 20 μg mL^{-1} ILE groups) (Fig. 5a). Contrastingly, the
189 proteolytic function of multiple mutant ClpC1P1P2 complexes was unaffected at 10 μg
190 mL^{-1} ILE compared to the control with $P > 0.05$, while some inhibition was noted at 20
191 μg mL^{-1} ILE with $P < 0.01$ (Fig. 5c-5f). For the ClpXP1P2 complex, ILE did not affect
192 its proteolytic activity (Fig. 5b). Although ILE did not affect the ATPase activity of
193 ClpX and the hydrolytic activity of ClpXP1P2, it may have other ways of exerting its
194 antimicrobial effects through ClpX or ClpXP1P2, which need to be explored further.

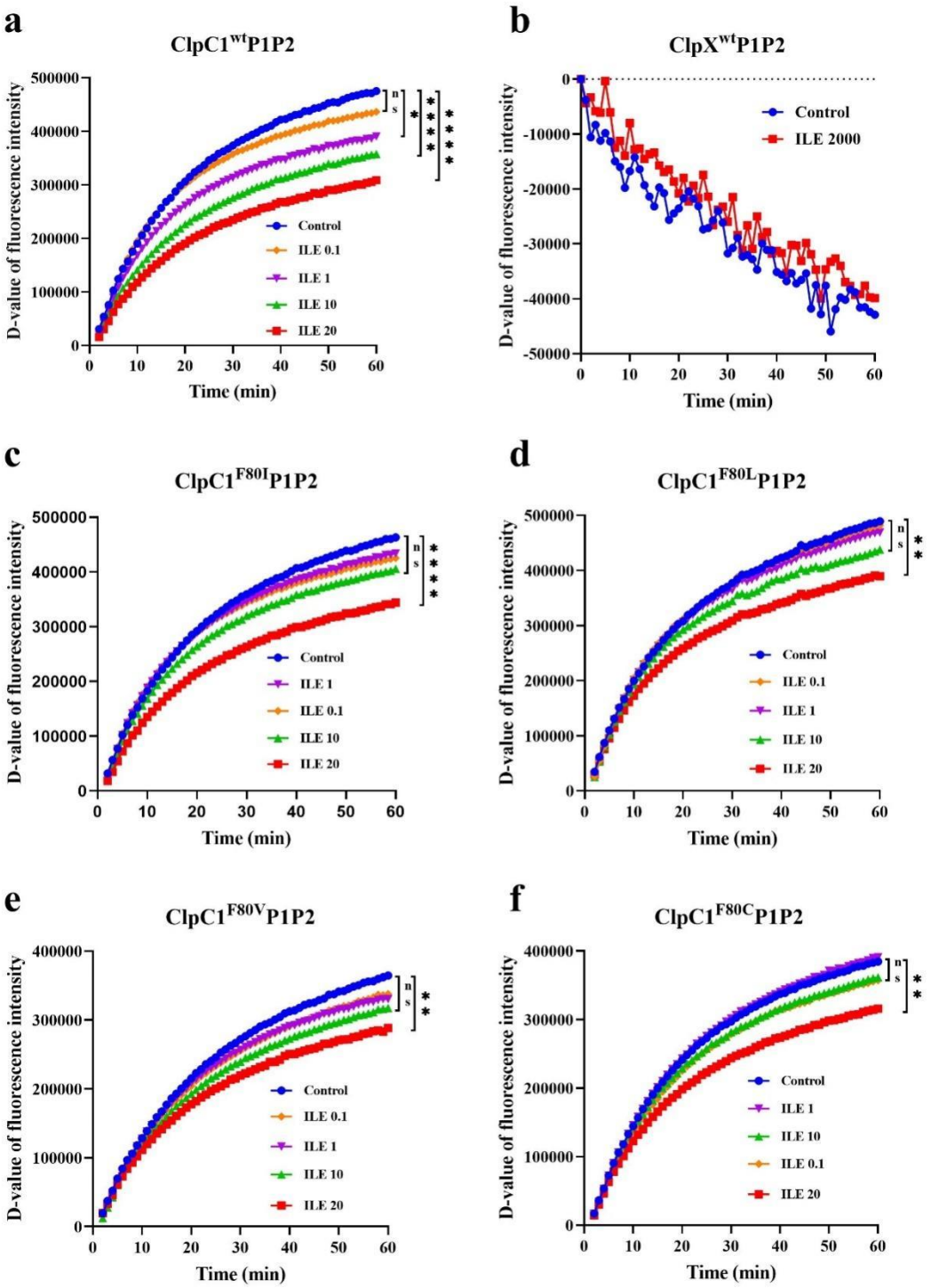

Fig. 5 | Proteolytic activity of the ClpC1P1P2 and ClpXP1P2 complexes in response to ILE treatment. a, c-f Proteolytic activity of variant ClpC1P1P2 complexes in response to ILE treatment. **b** Proteolytic activity of the ClpXP1P2 complexes in response to ILE treatment. ClpC1^{wt}P1P2, ClpC1^{F80I}P1P2, ClpC1^{F80L}P1P2, ClpC1^{F80V}P1P2, ClpC1^{F80C}P1P2: complex formation of wild-type and mutant ClpC1 with ClpP1 and ClpP2. ClpXP1P2: complex formation of wild-type ClpX with

ClpP1 and ClpP2. *: $P < 0.05$; **: $P < 0.001$; ****, $P < 0.00001$; ns, no significant difference, $P > 0.05$. Numbers after the drug names indicate the working concentrations (μg mL^{-1}). D-value of fluorescence intensity represents the change in fluorescence intensity by subtracting the fluorescence intensity of the first detection from the fluorescence intensity of each detection.

Extension of cell lengths and inhibition of cell division in ILE- and ILF-treated Msm

After treating with 0.125 μg mL^{-1} of ILE or 5 μg mL^{-1} of ILF for 15 h, the cell lengths of Msm (2.07 ± 0.48 μm) were extended to 5.95 ± 2.16 μm and 9.41 ± 2.40 μm, respectively (Fig. 6). This morphological change indicates an inhibition of cell division, as evidenced by the readily observable increase in division septa formation.

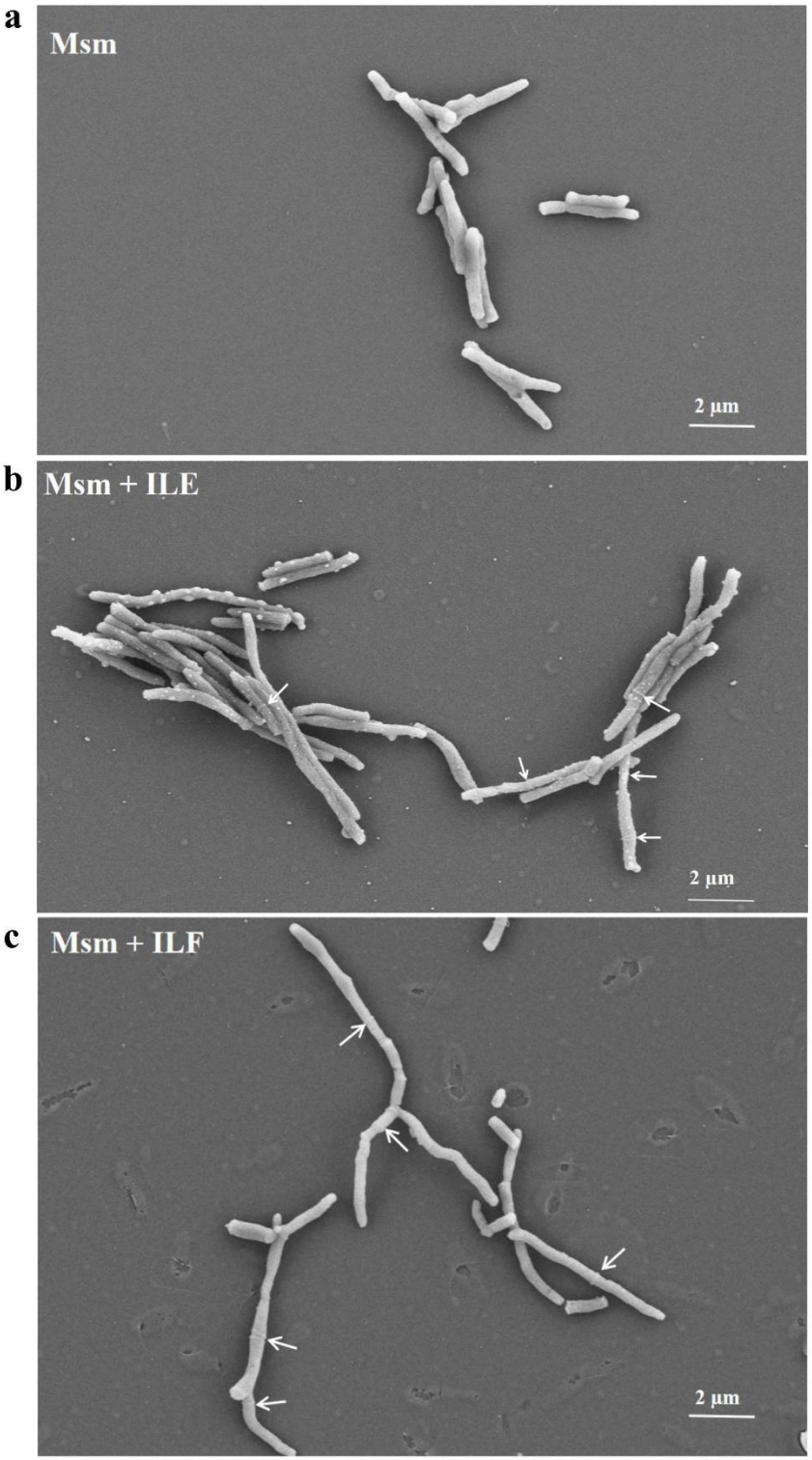

Fig. 6 | Cell morphology of Msm strains before or after treatment with ILE or ILF. a Cell morphology before treatment. **b** Cell morphology of 0.125 μg mL^{-1} ILE-treated Msm. **c** Cell morphology of 5 μg mL^{-1} ILF-treated Msm. White arrows indicate division septa.

Proteomic signature of the ILE-treated cells

Proteomic analysis was performed to provide insights into the adaptive responses of Mtb during ILE treatment to better understand the mechanism of action of ILE. Compared to untreated cells, ILE-treated Mtb displayed upregulation of proteins involved in protein synthesis, including various 50S and 30S ribosomal proteins, except for RplR and RpsC, which were downregulated. Regulatory sigma factors such as SigE, SigB, and SigL, crucial for gene transcription and translation, were also affected.

Intriguingly, components of the toxin-antitoxin system, including anti-sigma factors Rv3221A and Rv0516c, as well as toxins Rv0660c and Rv0748, were upregulated upon ILE treatment. This observation aligns with reports that some toxin-antitoxin proteins are targets of the ClpXP1P2 complex[14]. Correspondingly, ClpX was found to be downregulated, potentially leading to increased levels of toxin-antitoxin proteins and contributing to the altered cell morphology in ILE-treated Mtb.

Membrane protein expression was notably affected, with some increasing expression while others decreasing. Proteins implicated in intermediary metabolism and respiration, such as QcrA, QcrB, and CydD, were downregulated, hinting at the impact of ILE on respiratory pathways. Alterations in lipid metabolism-related proteins, including upregulation of FadE9, FadE29, and FadD24 and downregulation of FadD9, FadE6, FadE12, and FadE24, were also observed. Additionally, many membrane proteins (e.g., MmpL2, EccD5, EccE2) showed significant expression changes, while others like MmpS3, SecF, and TatA were downregulated in the presence of ILE.

Discussion

This study describes ILE and ILF, two cyclic peptides with potent anti-mycobacterial properties, isolated from a deep South China Sea-derived strain, *Streptomyces atratus* SCSIO ZH16[15]. Both ILE and ILF exhibited significant activity against Msm, Mmr, and Mtb, with ILE also effective against various drug-resistant clinical Mtb isolates. This suggests that ILE targets molecular mechanisms distinct from those drugs of current TB therapeutics. Additionally, ILE showed robust antibacterial activity against Mab. In mouse macrophages, ILE also has potent bactericidal activity. Notably, neither ILE nor ILF affected certain non-mycobacterial pathogens, such as *Staphylococcus aureus* and *Acinetobacter baumannii*, indicating a mycobacteria-specific action. This specificity mirrors that of other cyclic peptides like rufomycin I, lassomycin, ecumicin, and cycolmycin A, which also selectively target mycobacteria over common Gram-negative and Gram-positive bacteria, including *Escherichia coli* (*E. coli*) and *Staphylococcus aureus*[12,27-29].

Combination studies of ILE and ILF with various anti-TB drugs, including RIF, INH, STR, EMB, and TB47 revealed synergistic or additive interactions, except for an indifferent response with ILF + RIF. These results suggest the potential of ILE and ILF to enhance the efficacy of existing anti-TB therapies. Interestingly, our proteomic analysis revealed changes in four proteins associated with the mechanism of INH after ILE treatment, potentially explaining the synergistic effect of ilamycins with INH. Specifically, SigL (fold change > 28, $P < 0.01$) and Ndh (fold change = 4.79, $P < 0.001$) were significantly upregulated, while FadE24 (fold change = 0.35, $P < 0.5$) and Glf (fold change = 0.33, $P < 0.01$) were downregulated. SigL has been reported to activate KatG, which is critical for the effect of INH[30,31], while Ndh influences the $NADH/NAD^+$ ratio, affecting INH-NAD formation[32]. FadE24 was reported to be upregulated in the prescence of INH, and mutations in it have also been found in INH-resistant Mtb[33]. Glf is responsible for catalyzing the conversion of UDP-galactopyranose to UDP-galactofuranose. Its upregulation was hypothesized to contribute to INH resistance in Mtb either by binding a modified form of INH or by

265 sequestering a factor such as NAD^+ required for INH activity[34]. Additionally, crucial
266 proteins in the electron transport chain of Mtb such as QcrA, QcrB, and CydD were all
267 downregulated after treatment of ILE. Given the mutual substitutability of the two
268 electron transfer chains , it was previously speculated that the inhibitory effect of the
269 QcrB inhibitor TB47 on Mtb would be enhanced when cyt-bds is inhibited[24]. Therefore,
270 the downregulation of these proteins may explain its synergistic effect with ilamycins.

271 WGS and Sanger sequencing of spontaneous mutants resistant to ILE or ILF
272 identified ClpC1 as the primary target in Mtb, Mab, Msm, and Mmr. The mutations in
273 ClpC1 associated with ILE or ILF resistance mirror those reported in mutants resistant
274 to other ClpC1-targeting compounds. For instance, rufomycin I-resistant mutants
275 exhibited V13F, H77R, F80I/V/L/S mutations[27]; lassomycin-resistant strains harbored
276 Q17R/H, R21S, P79T mutations[29]; cyclomarin A-resistant variants showed F2A/Y,
277 F80A/Y, E89A/Q alterations[12]; and ecumicin resistance was linked to L92S/F, L96P
278 mutations[28]. Interestingly, all of these mutations were located in the MtbClpC1-NTD
279 (residues 1–145). However, no mutation was observed in ClpX of rufomycin I-,
280 lassomycin-, cyclomarin-, and ecumicin-resistant mutants[27-29,35]. On the other hand,
281 ILE-resistant mutants conferred ClpX mutations and also exhibited cross-resistance to
282 ILF, suggesting that ilamycins may interact with multiple targets within the
283 mycobacterial proteolytic machinery.

284 Molecular docking simulations elucidated the interactions between ILE and
285 MtbClpC1-NTD, as well as MtbClpX-NTD. These simulations identified key residues
286 such as Q17, H77, F80, and L88 in MtbClpC1-NTD, and P30 in MtbClpX-NTD that
287 consistent with sites of mutation in resistant strains. Comparable docking studies with
288 cyclic peptides rufomycin, ecumicin, and cyclomarin A against MtbClpC1-NTD
289 corroborated that these crucial residues align with mutation sites previously identified[36].
290 This consistency reinforces the relevance of these residues in the binding and efficacy
291 of anti-mycobacterial cyclic peptides.

292 Comparative analysis of Ilamycin-resistant mutants and gene-edited strains
293 suggests that mutations at the F2 position of ClpC1 in both Mab and Msm confer
294 relatively low-level resistance to ilamycins. Contrastingly, P30 mutations in Mab ClpX

295 correlate with high-level resistance in Mab, signifying its critical role. Notably, the lack
296 of impact of Msm *clpC1*^{I197N} mutation on ilamycin resistance is attributed to its location
297 outside the NTD of ClpC1, suggesting that resistance is primarily driven by alterations
298 within the NTD. Additionally, the mutant strain harbored this mutation also harbored a
299 mutation in F2 in ClpC1 which may mainly contribute to the resistance to ilamycins.
300 Overexpression studies further revealed that AlMmr strains overexpressing *clpC1*^{L88R}
301 exhibited resistance to ILE and ILF, paralleling previous observations of mutant *clpC1*
302 gene overexpression conferring resistance to ClpC1-targeting compounds. For example,
303 Msm strains expressing *clpC1*^{F80Y} and *clpC1*^{F89Y} mutants and *Mycobacterium bovis*
304 BCG strains expressing *clpC1*^{F2Y}, *clpC1*^{F80Y}, and *clpC1*^{E89A} mutants showed
305 statistically significant resistance ($P < 0.05$) to cyclomarin A compared with parent
306 strains[35]. Conversely, most overexpressed strains did not demonstrate drug resistance.
307 As both proteins ClpX and ClpC1 are used to regulate protein degradation, we
308 hypothesized that the proteins produced by overexpression are likely to be bound by
309 some proteins within the bacteria, rendering them non-functional or directly degraded,
310 so that most of the overexpression strains do not develop drug resistance. Moreover,
311 knockdown of *clpX* or *clpC1* genes heightened sensitivity to ilamycins in Mab and Msm,
312 also impacting strain growth, consistent with the essential nature of these genes for
313 mycobacterial viability[25,26]. Additionally, although sgRNAs in our study intended to
314 target the same site in *clpC1* and *clpX* in Mab and Msm, we observed that the effective
315 dose of aTc in Mab is evidently higher than in Msm, which may be due to the intrinsic
316 resistance of Mab towards tetracyclines by overexpression of a tetracycline-degrading
317 enzyme MabTetX (MAB_1496c)[37]. Collectively, these gene-level investigations
318 substantiate ClpX and ClpC1 as molecular targets of ILE and ILF, providing valuable
319 insight into their mechanism of action.

320 DSF analyses confirmed that both ILE and ILF enhance the thermal stability of
321 MtbClpC1-NTD with ILE showing a stronger affinity than ILF, which correlates with
322 its lower MIC. Unlike ecumicin and lassomycin, which stimulate ClpC1 ATPase
323 activity but impede substrate degradation, or cyclomarin A, which activates both
324 ATPase and proteolytic functions[27-29], ILE does not alter the ATPase activities of ClpX

325 and ClpC1. Instead, ILE inhibits the proteolytic activity of the ClpC1P1P2 complex
326 without affecting ATPase activities of ClpC1, suggesting a distinct mechanism that
327 disrupts protein homeostasis and leads to bacterial cell death. Although ILE had no
328 effect on the ATPase activity of ClpX and the hydrolytic activity of ClpXP1P2, it may
329 have other ways of exerting its antimicrobial effects through ClpX or ClpXP1P2, which
330 further need to be explored.

331 Scanning electron microscopy revealed that ILE and ILF treatments impede cell
332 division in Msm, consistent with the phenotype of *clpX* gene silencing[26]. This is also
333 consistent with the role of ClpX in regulating FtsZ assembly and Z-ring formation,
334 essential for cell division in Mtb[38]. Proteomic data further indicated that ILE markedly
335 increases toxin and antitoxin protein expression, known substrates of the ClpXP1P2
336 complex[14], hinting at a potential targeting of ClpX by ilamycins.

337 Future studies should focus on specifying the precise interactions between
338 ilamycins, ClpX, and the ClpXP1P2 complex to fully understand the mechanism. The
339 collective evidence from this and related studies[27-29,35] establishes ClpC1 and ClpX as
340 promising targets for TB therapy.

341 # Methods

342 **Bacterial strains and media**

343 Bacterial strains used in this study are listed in Supplementary Table 1. For Mtb,
344 Mmr, Mab, and Msm, cells were grown in Middlebrook 7H9 broth supplemented with
345 OADC (0.005% oleic acid, 0.5% bovine serum albumin, 0.2% dextrose, 0.085%
346 catalase). For *E. coli*, *Enterococcus faecium*, *Staphylococcus aureus*, *Acinetobacter*
347 *baumannii*, *Klebsiella pneumoniae* and *Pseudomonas aeruginosa*, cells were grown in
348 Luria-Bertani (LB) broth.

349 **MICs against mycobacteria**

350 The MICs of ILE and ILF were detected using a cost-effective *in vitro* assay as
351 previously described against a selectable marker-free autoluminescent Mtb $H_{37}Ra$
352 (AlRa), AlRv, AlMab, AlMsm and AlMmr[22-24,39]. In such cases, the MIC_{lux} was defined
353 as the lowest concentration that can inhibit > 90% relative light units (RLUs) compared
354 with that from the untreated controls[22-24,39]. The MICs of the ILE were also determined
355 by a well-established microplate alamar blue assay (MABA) against Mtb $H_{37}Ra$, $H_{37}Rv$
356 and nine clinical Mtb strains isolated from pulmonary TB patients hospitalized in
357 Guangzhou Chest Hospital, Guangzhou, China[20,31]. The MIC by MABA method was
358 defined as the lowest concentration corresponding to the blue column on the microplate
359 was observed by naked eye.

360 **MICs against non-mycobacteria**

361 The MICs against *Enterococcus faecium*, *Staphylococcus aureus*, *Acinetobacter*
362 *baumannii*, *Klebsiella pneumoniae* and *Pseudomonas aeruginosa* were determined by
363 observing the turbidity after 16 h of incubation in LB broth at 37℃. The MIC was
364 defined as the lowest concentration, resulting in clarity in turbidity relative to that of
365 untreated control cultures[40,41].

366 **Combined activity of ILE or ILF with other compounds *in vitro***

367 The combined activity of ILE or ILF with INH, RIF, EMB, STR and TB47 was
368 tested by a checkerboard method. The fractional inhibitory concentration index (FICI)

369 was interpreted as follows: synergistic (FICI of ≤ 0.5), partially synergistic (0.5 < FICI
370 < 1.0), additive (FICI = 1.0), indifferent (1.0 < FICI ≤ 4.0), and antagonistic (FICI >
371 4.0)[42,43].

372 **Activity in macrophage culture**

373 The growth inhibition of AlRv in macrophage culture was assessed as previously
374 described[42]. The cell density of mouse macrophages RAW264.7 was adjusted to 5×10^5
375 cells mL^{-1}. 100 μL cells per well were added to 96-well plates and cultured overnight
376 for adherence. The AlRv was adjusted to 3×10^6 RLU mL^{-1}, and 100 μL AlRv was
377 added to each well. The plates were then incubated at 37℃ for 6 h. The cells were
378 washed three times with DMEM to remove the AlRv that was not phagocytosed and
379 treated with DMEM containing amikacin (100 μg mL^{-1}) for 2 h to eliminate the
380 extracellular bacteria. The cells were washed twice with DMEM to remove any residual
381 amikacin. A total of 195 μL of DMEM containing 10% fetal bovine serum and 5 μL of
382 the two-fold dilutions of different ILE concentrations were added to the cells. The
383 mixture was incubated at 37℃ with 5% CO_2 and the RLUs were measured on days 1-
384 5 or 7 of incubation. RIF (1 μg mL^{-1}) and dimethyl sulfoxide (DMSO) were used as
385 positive and negative controls, respectively.

386 **ILE or ILF-resistant mutants**

387 Broth cultures of AlRa, AlRv, AlMab, and AlMmr, having OD_{600} 0.6-1.3, were
388 plated on 7H11 plates containing 0.1, 0.5, 2.5, 5, 10 or 20 μg mL^{-1} of ILE. Broth cultures
389 of AlMsm (OD_{600} 0.6-1.3) were plated on 7H11 plates containing 10, 20 or 40 μg mL^{-1}
390 of ILF. The bacterial colonies grown on the ILE- or ILF-containing plates were picked
391 up to confirm the drug resistance phenotype by drug susceptibility testing in liquid
392 culture.

393 **WGS analysis**

394 The whole-genomes of the parent Mtb, Mab and a part of the confirmed ILE-
395 resistant mutants were sequenced by the Beijing Genomics Institute in China. The
396 resulting reads were aligned to the reference genome sequence and compared with that
397 of the parent strain. The mutations identified by WGS analysis in the drug-resistant

398 mutants were verified by amplifying and sequencing the *clpX* and *clpC1* genes by
399 Sanger sequencing. The *clpX* and *clpC1* genes of other ILE- or ILF-resistant mutants,
400 including Mtb, Mab, Msm, and Mmr, were amplified and detected by Sanger
401 sequencing (primers are listed in Supplementary Table 2).

402 **Molecular docking analysis**

403 To assess the binding affinities and interaction modes among ILE, MtbClpC1-
404 NTD, and MtbClpX-NTD, Autodock Vina 1.2.2, a computational protein–ligand
405 docking software, was utilized[44]. The structure of ILE was obtained from PubChem
406 Compound[45]. The 3D coordinates of MtbClpC1-NTD (PDB code, 6CN8; resolution,
407 1.4 Å) were retrieved from the Protein Data Bank (PDB), and the structure of MtbClpX-
408 NTD was predicted using AlphaFold2.

409 For the docking analysis, all protein and molecular files were converted to the
410 PDBQT format, excluding water molecules, and polar hydrogen atoms were added. The
411 grid box was centered to encompass the domain of each protein, allowing for free
412 molecular movement. The dimensions of the grid box were set to 30 Å × 30 Å × 30 Å,
413 with a grid point distance of 0.05 nm. Molecular docking studies were conducted using
414 Autodock Vina 1.2.2, available at http://autodock.scripps.edu/.

415 **Overexpression of *clpX* or *clpC1* in Mab, Mmr or Msm**

416 $clpC1^{wt}$, $clpC1^{mt}$ (mutated *clpC1*), $clpX^{wt}$ and $clpX^{mt}$ from Mtb, Mab, Mmr and
417 Msm were amplified (primers are listed in Supplementary Table 2) and cloned into the
418 plasmid p60A or pMVA with high copies under the control of the *hsp60* promoter
419 (Supplemantary Fig. 1)[24]. The plasmids were transformed into AlMab, AlMmr, and
420 AlMsm. Furthermore, the *clpP1*, *clpP2* and *clpX* or *clpC1* of Mab were amplified from
421 the genome of Mab^{wt} and inserted into the plasmid pMVA under the control of the *hsp70*
422 and *hsp60* promoters for expressing ClpXP1P2 or ClpC1P1P2 simultaneously. The
423 MICs of the recombinant strains to ILE or ILF were determined as described above.

424 **Gene silencing of *clpX* or *clpC1* genes in Mab or Msm**

425 CRISPR interference was used to perform *clpX* or *clpC1* gene silencing[46]. 20-bp-
426 long oligonucleotides were designed as sgRNA to bind the sense strand of the coding

region of *clpX* or *clpC1*. The oligonucleotides were annealed and then ligated with linearized pLJR962[46]. Subsequently, the empty vector pLJR962 and the plasmids containing sgRNAs targeting *clpX* or *clpC1* (Supplemantary Table 3) separately were electroporated into receptive cells of Mab or Msm. The gene-silenced strains and the empty vector transformant were cultured and the gene-silencing effects were determined. 4 μL ILE was added to the 96-well microplate making the final concentration of 8 ~ 0.0313 μg mL^{-1}. The concentration of bacteria, whose OD_{600} were adjusted to ~ 0.5, was 1000-fold diluted in 7H9 with or without aTc. The diluted bacteria were then divided into the experimental group (+ aTc 50 ng mL^{-1}) and the control group (- aTc). 196 μL of these two groups were then inoculated into the 96-well microplate separately. The microplates were incubated at 37°C for 3 days. The MIC was defined as the lowest concentration that prevented visible bacterial growth. The experiment was performed in triplicate and repeated twice.

Ten-fold serial dilutions of Mab^{wt} or Msm^{wt}, the empty vector transformant, and the gene-silenced strains were prepared after adjusting OD_{600} to ~0.9. For Mab, 1 μL of each dilution was spotted on plates containing 0.25, 0.5, and 1 μg mL^{-1} ILE or 5, 10, and 20 μg mL^{-1} with different concentrations of aTc (0, 100, 200 and 400 ng mL^{-1}). For Msm, 1 μL of each dilution was spotted on plates containing 0.004, 0.008, and 0.01625 μg mL^{-1} ILE or 0.125, 0.25, and 0.5 μg mL^{-1} ILF with different concentrations of aTc (0, 12.5, 25 and 50 ng mL^{-1}). As a control, 1 μL of each dilution was also spotted on plates containing only aTc. The plates were incubated at 37℃ for 3 days. The experiment was performed in triplicate and repeated twice.

CRISPR/Cpf1-mediated gene editing of *clpX* and *clpC1* genes in Mab and Msm

The CRISPR/Cpf1-associated recombination have been used for gene editing in Mab and Msm previously[20,21]. Firstly, the pJV53-Cpf1 was electroporated into Mab^{wt} and Msm^{wt} for the Mab::pJV53-Cpf1 and Msm::pJV53-Cpf1. Secondly, sgRNAs were designed to target 25 nucleotide sequences, which followed the sequence 5'-YTN-3' on the template strand of each target gene (Supplementary Table 3). All oligonucleotides designed for sgRNA expression were ligated into pCR-zeo. Subsequently, the vectors

456 were electroporated into receptive cells of induced Mab::pJV53-Cpf1 or Msm::pJV53-
457 Cpf1. For Cpf1 expression, aTc was added to 7H11 agar plates at a final concentration
458 of 200 ng mL^{-1}. These plates were cultured in 30°C incubators for 3-5 days, and then
459 single colonies were selected to determine whether the site of the target gene had been
460 edited successfully by PCR and Sanger sequencing (primers are listed in
461 Supplementary Table 2). The MICs of the edited strains to ILE and ILF were tested as
462 described above.

463 **Protein expression and purification**

464 Mtb ClpP1 (residues 7-200) and ClpP2 (residues 13-214) with N-terminal His_6-
465 SUMO tags were expressed and purified. In short, ClpP1 and ClpP2 were individually
466 overexpressed in *E. coli* BL21 (λDE3) in LB broth at 16°C, following induction with
467 0.5 mM isopropyl β-D-1-thiogalactopyranoside (IPTG) for approximately 16 h. Cells
468 were resuspended and lysed; His-tagged ClpP1/ClpP2 proteins were subsequently
469 purified via nickel affinity chromatography and eluted with the same buffer
470 supplemented with 250 mM imidazole. The His_6-SUMO tag of eluted proteins was
471 removed by ubiquitin-like-protease 1 at 4°C. Following the purification of the tag-free
472 proteins, peak fractions were collected and concentrated through anion exchange
473 chromatography (MonoQ; GE Healthcare). These fractions were then applied to
474 Superdex 200 16/600 (GE Healthcare) for final purification. ClpP1 and ClpP2 were
475 then concentrated in amicon centrifugal concentration devices (Millipore) to a
476 tetradecamer concentration of more than 80 μM.

477 $clpX^{wt}$ and $clpX^{P30H}$ were inserted into the pGEX-6P-1 vector, which had a His_6-
478 tag at the C-terminal and an HRV 3C protease cleavage site. After induction for 18 h at
479 16°C, the cells were collected by centrifugation. The pellet was then resuspended and
480 lysed. After centrifugation, the supernatant was loaded onto a GST column and eluted.
481 The eluent was digested at 4°C for 26 h with enough HRV 3C protease. The fractions
482 containing the target protein were then pooled, concentrated to 1 mL, and purified with
483 a SuperoseTM 6 increase 10/300 GL column.

484 $clpC1^{wt}$, its mutants (F80I/V/L/C), and *gfp*-ssrA (AGKEKQNLAFAA) were

485 inserted into the pET-28a vector that had an N-terminal His_6-tag. The recombinant
486 strains were cultured in LB broth at 37°C until OD_{600} reached 0.6-0.8. After 18 h of
487 induction with 0.5 mM IPTG at 18°C, the pellet was suspended and lysed. Following
488 the loading of the supernatant onto a Ni-NTA column, the proteins were washed and
489 then eluted. The fractions were then pooled and loaded onto a SuperoseTM 6 increase
490 10/300 GL column.

491 The coding gene sequence of MtbClpC1-NTD (residues 1–145) and MtbClpX-
492 NTD (residues 1–112) were inserted into the pET-28a vector with a C-terminal His_6-
493 tag and an HRV 3C protease cleavage site. The expression and purification methods of
494 MtbClpC1-NTD and MtbClpX-NTD were consistent with the above methods.

495 **DSF**

496 DSF was used to detect ILE or ILF binding to the MtbClpC1-NTD and MtbClpX-
497 NTD based on the established methods[47 48]. 5 μM MtbClpX-NTD or MtbClpC1-NTD
498 was incubated with different concentration of ILE or ILF (range from 12.5 to 400 μM)
499 or DMSO for 0.5 h, then mixed with Sypro Orange fluorescent dye. The fluorescence
500 readings were observed using the CFX96 Real-time System (Bio-rad), in which the 8-
501 tube PCR Strips were smoothly heated from 25°C to 95°C at a constant heating rate of
502 0.4°C min^{-1}. The excitation and emission filters were set at $\lambda = 460$ nm and $\lambda = 510$ nm,
503 respectively. The data were collected with CFX Manager software and analyzed using
504 GraphPad Prism 8.0.2. All measurements were carried out in triplicate.

505 **ClpC1 and ClpX ATPase activity assay**

506 The ATPase activity of Mtb ClpC1 and ClpX was assessed via a free-phosphate
507 detection assay using the Biomol Green reagent. 5 μL of various concentrations of ILE
508 (0, 0.08, 0.16, 0.31, 0.625, 1.25, 2.5, 5 and 10 μg mL^{-1}) was added to each well of a
509 transparent 96-well plate. The ClpX or ClpC1 were diluted to 0.1 μg mL^{-1} in the reaction
510 mixture. 90 μL ClpC1 and ClpX were added to a 96-well plate and incubated at 37°C
511 for 1 h. The reaction was initiated by adding 5 μL of 1 mM ATP to the reaction mixture
512 at 37°C for 1 h. The final volume of the reaction mixture was adjusted to 100 μL. After
513 the reaction, 100 μL of Biomol Green reagent was added to determine the amount of

514 free phosphate. After incubation at room temperature for 30 min, the resulting reaction
515 product was measured at 620 nm using a Multimode Plate Reader (Envision,
516 PerkinElmer, USA). The concentration of free phosphate released from ATP by ClpX
517 and ClpC1 was calculated using a standard curve according to the concentration of free
518 phosphate. Measurements were performed in triplicate.

519 **Proteolytic activity assay of ClpC1P1P2 and ClpXP1P2**

520 The proteolytic activity of ClpC1P1P2 and ClpXP1P2 were measured at 37℃ in
521 white 96-well plates using a Multimode Plate Reader (Envision, PerkinElmer, USA).
522 ILE was added at 0, 0.1, 1, 10, and 20 μg mL^{-1} as the final concentrations in each well
523 of a white 96-well plate. 100 μL reaction mixture was prepared as 2 μM ClpP1P2, 1
524 μM ClpC1 or ClpX, and 2.5 μM fluorescein isothiocyanate (FITC)-casein for
525 ClpC1P1P2 or 2 μM GFP-SsrA for ClpXP1P2. The FITC-casein and GFP-SsrA
526 hydrolysis was continuously monitored at 535 nm (excitation at 485 nm).
527 Measurements were performed in triplicate.

528 **Microscopy of ILE- or ILF-treated Msm**

529 We treated exponentially growing Msm with 0.125 μg mL^{-1} ILE or 5 μg mL^{-1} ILF
530 for 15 h. The bacteria immobilized by 4% glutaraldehyde were washed three times and
531 resuspended with phosphate-buffered saline (PBS). 5 mm cell slides were soaked in
532 bacterial suspension and placed in a 24-well plate for drying naturally. Subsequently,
533 the cell slides were washed three times with PBS. Successive soaks with gradually more
534 concentrated (70%, 80%, 90%, 100%) ethanol solutions were performed for 10 minutes
535 each. Cell slides were dried using the critical point drying method and then coated with
536 electrically-conducting material. The bacterial morphology was observed by a
537 GeminiSEM 300 ultra-high resolution field emission cryo-scanning electron
538 microscope.

539 **Proteomic analysis**

540 AlRa was treated for 5 days, in triplicate, with 0.0125 μg mL^{-1} ILE for 4D label-
541 free phospho-proteomic analysis. The untreated cells were diluted on the same day, and
542 the compounds were added to reach a comparable cell density between untreated and

ILE-treated cells before sample collection. The cells were resuspended and boiled for 20 min. The samples were then sent to APTBIO (Shanghai, China) for proteomics testing and analysis.

To compare the abundance of phosphopeptides between the control and treatment samples, label-free quantification was performed with a minimum fold change of 1.5 to determine the differentially expressed phosphopeptides. In addition, the student's *t-test* was employed to identify significant differences between the control and treatment samples. $P < 0.05$ were considered to indicate significance. Functional category analysis was conducted according to Mycobrowser (https://mycobrowser.epfl.ch/). Protein functional annotation was performed with DAVID (https://david.ncifcrf.gov/summary.jsp).

Statistical analysis

Statistical analysis was performed with GraphPad Prism 8.0.2. The unpaired *t-test* was applied to determine statistical significance. $P < 0.05$ was considered significant.

557 ## References

558 1. Bouzeyen R, Javid B. Therapeutic vaccines for tuberculosis: An overview. *Front*
559 *Immunol* **13**, 878471 (2022).
560 2. Miotto P, Zhang Y, Cirillo DM, Yam WC. Drug resistance mechanisms and drug
561 susceptibility testing for tuberculosis. *Respirology* **23**, 1098-1113 (2018).
562 3. Pfyffer G. Drug-resistant tuberculosis: resistance mechanisms and rapid
563 susceptibility testing. *Schweiz med Wochenschr* **130**, 1909-1913 (2000).
564 4. Fedrizzi T*, et al.* Genomic characterization of nontuberculous mycobacteria. *Sci*
565 *rep* **7**, 45258 (2017).
566 5. Henkle E, Winthrop KL. Nontuberculous mycobacteria infections in
567 immunosuppressed hosts. *Clin chest med* **36**, 91-99 (2015).
568 6. Fraga H*, et al.* Development of high throughput screening methods for inhibitors
569 of ClpC1P1P2 from *Mycobacteria tuberculosis*. *Anal Biochem* **567**, 30-37
570 (2019).
571 7. Lupoli TJ, Vaubourgeix J, Burns-Huang K, Gold B. Targeting the proteostasis
572 network for mycobacterial drug discovery. *ACS infect dis* **4**, 478-498 (2018).
573 8. Lee H, Suh JW. Anti-tuberculosis lead molecules from natural products targeting
574 *Mycobacterium tuberculosis* ClpC1. *J Ind Microbiol Biotechnol* **43**, 205-212
575 (2016).
576 9. d'Andrea FB, Poulton NC, Froom R, Tam K, Campbell EA, Rock JM. The
577 essential *M. tuberculosis* Clp protease is functionally asymmetric *in vivo*. *Sci Adv*
578 **8**, eabn7943 (2022).
579 10. Raju RM*, et al. Mycobacterium tuberculosis* ClpP1 and ClpP2 function together
580 in protein degradation and are required for viability *in vitro* and during infection.
581 *PLoS pathog* **8**, e1002511 (2012).
582 11. Akopian T, Kandror O, Raju RM, UnniKrishnan M, Rubin EJ, Goldberg AL. The
583 active ClpP protease from *M. tuberculosis* is a complex composed of a
584 heptameric ClpP1 and a ClpP2 ring. *EMBO J* **31**, 1529-1541 (2012).
585 12. Schmitt EK*, et al.* The natural product cyclomarin kills *Mycobacterium*

586 *tuberculosis* by targeting the ClpC1 subunit of the caseinolytic protease. *Angew*
587 *Chem Int Ed Engl* **50**, 5889-5891 (2011).
588 13. Sassetti CM, Boyd DH, Rubin EJ. Genes required for mycobacterial growth
589 defined by high density mutagenesis. *Mol Microbiol* **48**, 77-84 (2003).
590 14. Texier P*, et al.* ClpXP-mediated degradation of the TAC antitoxin is neutralized
591 by the SecB-like chaperone in *Mycobacterium tuberculosis*. *J Mol Biol* **433**,
592 166815 (2021).
593 15. Ma J*, et al.* Biosynthesis of ilamycins featuring unusual building blocks and
594 engineered production of enhanced anti-tuberculosis agents. *Nat Commun* **8**, 391
595 (2017).
596 16. Gutiérrez AV, Viljoen A, Ghigo E, Herrmann J-L, Kremer L. Glycopeptidolipids,
597 a double-edged sword of the *Mycobacterium abscessus* complex. *Front*
598 *microbiol* **9**, 1145 (2018).
599 17. Jankute M, Grover S, Birch HL, Besra GS. Genetics of mycobacterial
600 arabinogalactan and lipoarabinomannan assembly. *Molecular Genetics of*
601 *Mycobacteria*, 535-557 (2014).
602 18. Lu XY*, et al.* Pyrazolo[1,5-]pyridine inhibitor of the respiratory cytochrome
603 complex for the treatment of drug-resistant tuberculosis. *Acs Infect Dis* **5**, 239-
604 249 (2019).
605 19. Bergval I*, et al.* Pre-existing isoniazid resistance, but not the genotype of
606 *Mycobacterium tuberculosis* drives rifampicin resistance codon preference *in*
607 *vitro*. *PLoS One* **7**, e29108 (2012).
608 20. Wang S*, et al.* Amino acid 17 in QRDR of gyrase A plays a key role in
609 fluoroquinolones susceptibility in mycobacteria. *Microbiol Spectr* **11**, e0280923
610 (2023).
611 21. Yan M-Y, Yan H-Q, Ren G-X, Zhao J-P, Guo X-P, Sun Y-C. CRISPR-Cas12a-
612 Assisted Recombineering in Bacteria. *Appl Environ Microbiol* **83**, (2017).
613 22. Liu Y*, et al.* Assessment of clofazimine and TB47 combination activity against
614 *Mycobacterium abscessus* using a bioluminescent approach. *Antimicrob Agents*
615 *Chemother* **64**, (2020).

616 23. Yang F, *et al.* Engineering more stable, selectable marker-free autoluminescent
617 mycobacteria by one step. *PloS One* **10**, e0119341 (2015).
618 24. Liu Y, *et al.* The compound TB47 is highly bactericidal against *Mycobacterium*
619 *ulcerans* in a Buruli ulcer mouse model. *Nat Commun* **10**, 524 (2019).
620 25. Rifat D, Chen L, Kreiswirth BN, Nuermberger EL. Genome-wide essentiality
621 analysis of *Mycobacterium abscessus* by saturated transposon mutagenesis and
622 deep sequencing. *mBio* **12**, e0104921 (2021).
623 26. Bai J, Chi M, Hu Y, Hao M, Zhang X. Construction and biological characteristics
624 of ClpC and ClpX knock-down strains in *Mycobacterium smegmatis*. *Chin. J.*
625 *Biotechnol* **41**, 13-22 (2021).
626 27. Choules MP, *et al.* Rufomycin targets ClpC1 proteolysis in *Mycobacterium*
627 *tuberculosis* and *M. abscessus*. *Antimicrob Agents Chemother* **63**, e02204-18
628 (2019).
629 28. Gao W, *et al.* The cyclic peptide ecumicin targeting ClpC1 is active against
630 *Mycobacterium tuberculosis in vivo*. *Antimicrob Agents Chemother* **59**, 880-889
631 (2015).
632 29. Gavrish E, *et al.* Lassomycin, a ribosomally synthesized cyclic peptide, kills
633 *Mycobacterium tuberculosis* by targeting the ATP-dependent protease
634 ClpC1P1P2. *Chem biol* **21**, 509-518 (2014).
635 30. Sklar JG, Makinoshima H, Schneider JS, Glickman MS. *M. tuberculosis*
636 intramembrane protease Rip1 controls transcription through three anti-sigma
637 factor substrates. *Mol microbiol* **77**, 605-617 (2010).
638 31. Hameed HA, *et al.* Molecular targets related drug resistance mechanisms in
639 MDR-, XDR-, and TDR-*Mycobacterium tuberculosis* strains. *Front cell infect*
640 *microbiol* **8**, 114 (2018).
641 32. Unissa AN, Subbian S, Hanna LE, Selvakumar N. Overview on mechanisms of
642 isoniazid action and resistance in *Mycobacterium tuberculosis*. *Infect Genet Evol*
643 **45**, 474-492 (2016).
644 33. Ramaswamy SV, *et al.* Single nucleotide polymorphisms in genes associated
645 with isoniazid resistance in *Mycobacterium tuberculosis*. *Antimicrob Agents*

646 *Chemother* **47**, 1241-1250 (2003).
647 34. Chen P, Bishai WR. Novel selection for isoniazid (INH) resistance genes
648 supports a role for NAD+-binding proteins in mycobacterial INH resistance.
649 *Infect Immun* **66**, 5099-5106 (1998).
650 35. Vasudevan D, Rao SP, Noble CG. Structural basis of mycobacterial inhibition by
651 cyclomarin A. *J Biol Chem* **288**, 30883-30891 (2013).
652 36. Wolf NM*, et al.* High-resolution structure of ClpC1-rufomycin and ligand
653 binding studies provide a framework to design and optimize anti-tuberculosis
654 leads. *ACS Infect Dis* **5**, 829-840 (2019).
655 37. Rudra P, Hurst-Hess K, Lappierre P, Ghosh P. High levels of intrinsic tetracycline
656 resistance in *Mycobacterium abscessus* are conferred by a tetracycline-modifying
657 monooxygenase. *Antimicrob Agents Chemother* **62**, e00119-18 (2018).
658 38. Dziedzic R*, et al. Mycobacterium tuberculosi*s ClpX interacts with FtsZ and
659 interferes with FtsZ assembly. *PloS One* **5**, e11058 (2010).
660 39. Zhang T, Li S-Y, Nuermberger EL. Autoluminescent *Mycobacterium*
661 *tuberculosis* for rapid, real-time, non-invasive assessment of drug and vaccine
662 efficacy. *PloS One* **7**, e29774 (2012).
663 40. Tian X*, et al.* Rapid visualized assessment of drug efficacy in live mice with a
664 selectable marker-free autoluminescent *Klebsiella pneumoniae*. *Biosens*
665 *Bioelectron* **177**, 112919 (2021).
666 41. Wang S*, et al.* Rapid, serial, non-invasive quantification of *Pseudomonas*
667 *aeruginosa* in live mice with a selectable marker-free autoluminescent strain.
668 *Biosens Bioelectron* **165**, 112396 (2020).
669 42. Yu W*, et al.* TB47 and clofazimine form a highly synergistic sterilizing block in
670 a second-line regimen for tuberculosis in mice. *Biomed pharmacother* **131**,
671 110782 (2020).
672 43. Liu P*, et al.* Design and synthesis of novel pyrimidine derivatives as potent
673 antitubercular agents. *Eur J Med Chem* **163**, 169-182 (2019).
674 44. Morris GM, Huey R, Olson AJ. Using autodock for ligand-receptor docking.
675 *Curr protoc bioinformatics* **24**, 8.14. 11-18.14. 40 (2008).

676 45. Wang Y, *et al.* Pubchem bioassay: 2017 update. *Nucleic Acids Res* **45**, D955-
677 D963 (2017).
678 46. Rock JM, *et al.* Programmable transcriptional repression in mycobacteria using
679 an orthogonal CRISPR interference platform. *Nat microbiol* **2**, 1-9 (2017).
680 47. Vivoli M, Novak HR, Littlechild JA, Harmer NJ. Determination of protein-
681 ligand interactions using differential scanning fluorimetry. *J Vis Exp*, e51809
682 (2014).
683 48. Khadiullina R, Mirgayazova R, Davletshin D, Khusainova E, Chasov V, Bulatov
684 E. Assessment of thermal stability of mutant p53 proteins via differential
685 scanning fluorimetry. *Life (basel)* **13**, 31 (2022).

686 **Acknowledgments**

687 We acknowledge the Yicheng Sun group from the Institute of Pathogenic Biology,
688 Chinese Academy of Medical Sciences for kindly sending the pJV53-Cpf1 and pCR-
689 Zeo plasmids as the tool of gene editing. This work was supported by the National Key
690 R&D Program of China (2021YFA1300900), the National Natural Science Foundation
691 of China (81973372, 32300152, 82022067, 22037006), China Postdoctoral Science
692 Foundation (2022M723164), Guangdong Provincial Basic and Applied Basic Research
693 Fund (2022A1515110505, 2019B030302004), the grant of State Key Lab of
694 Respiratory Disease (SKLRD-Z-202414, SKLRD-Z-202301), Open Program of Shen
695 Zhen Bay Laboratory (SZBL2021080601006) and Nansha District Science and
696 Technology Plan Project (NSJL202102). The funders had no role in study design, data
697 collection and analysis, decision to publish, or preparation of the manuscript.

698 **Author contributions**

699 T.Z., J.M, and X.X. supervised the project; T.Z., Y.G., and C.F. designed the whole
700 project and most of the experiments; J.M. and C.S. prepared and characterized the
701 ilamycin E and ilamycin F; Y.G. and C.F. performed the susceptibility testing and
702 resistant mutant screening; B.Z. and J.J. contributed to molecular docking simulation;
703 C.F., X.T. and J.H. constructed overexpression and gene-editing strains and peformed

704 the susceptibility testing; C.F. and X.H. performed the gene-scilencing experiments;
705 Y.G. and B.Z. contributed to protein expression and mode of action experiments; C.F.
706 and H.Z. contributed to the microscopy results; Y.G. performed the statistical analysis;
707 Y.G., F.C., and T.Z. wrote the manuscript; H.M.A., J.M., X.C., N.Z., X.X., J.J., and T.Z.
708 revised the manuscript.

709 Competing interests

710 The authors have no competing interests to declare that are relevant to the content of
711 this article.